A Journal of the Gesellschaft Deutscher Chemiker

Angewandte International Edition GDCh Chemie

www.angewandte.org

Accepted Article

Title: Multi-Dimensional Organic Mass Cytometry: Simultaneous Analysis of Proteins and Metabolites on Single Cells

Authors: Shuting Xu, Mingxia Liu, Yu Bai, and Huwei Liu

To be cited as: *Angew. Chem. Int. Ed.* 10.1002/anie.202009682

Link to VoR: https://doi.org/10.1002/anie.202009682

WILEY-VCH

10.1002/anie.202009682

WILEY-VCH

RESEARCH ARTICLE

Multi-Dimensional Organic Mass Cytometry: Simultaneous Analysis of Proteins and Metabolites on Single Cells

Shuting Xu, Mingxia Liu, Yu Bai,* and Huwei Liu

Abstract: Mass cytometry is attracting significant attention for its spatiotemporal high-throughput single-cell analysis. As the first demonstration of simultaneous detection of single-cell proteins and untargeted metabolites, a multi-dimensional organic mass cytometry system was established by a simple microfluidic chip connected to a nanoelectrospray mass spectrometer, providing useful cell heterogeneous information. A series of mass probes with online-dissociated mass tags were developed, ensuring the semi-quantification of cell surface proteins and compatibility of endogenous metabolite detection at single-cell level. Six cell surface antigens and ~100 metabolites from three ovarian cancer cell types and two breast cancer cell types were successfully monitored, and contributed to highly sensitive and specific cell typing. Doxorubicin-resistant cancer cell analysis confirmed its applications in distinguishing rare cell phenotypes. As a new generation of mass cytometry, the proposed system is simple, extensible, and promising for cell typing, drug-resistance analysis of tumor cells, and clinical diagnosis and therapy at single-cell level.

Introduction

The detection and understanding of individual cells within populations is fundamental to many basic biological processes such as differentiation, aging, and pathopoiesis.[1] Considering the limited size and extensive information of single cells from the cellular genome, transcriptome, and proteome to metabolome, technologies has surged towards single-cell-level sensitivity, high information coverage, and spatiotemporal high-throughput.[2] Compared to single-cell sequencing[3], single-cell proteome[4] and metabolome[5] are of great significance since they are the direct performers of vital movement and the final products and essential mediators of cellular behavior, respectively. Moreover, their detection is challenging because of their large diversity, low abundancy, and lack of amplification ability. High sensitivity and rich information have made mass spectrometry (MS) a powerful tool for protein and metabolite measurement in single cells.[4b, 5a, 6] The combination of MS and flow cytometry further promotes the temporal and spatial throughput, which was demonstrated by the cytometry by time-of-flight (CyTOF) based on inductively coupled plasma mass spectrometry (ICP-MS).[7] It achieves sufficient single-cell protein sensitivity through abundant heavy-metal isotopes chelated on antibodies,[8] and enables the rapid and simultaneous measurements of >40 parameters in many ground-breaking cell biology research,[9] which is unbeatable when compared to fluorescence-based flow cytometry. However, the high cost of limited isotopes and the specialized nature of elemental MS limit its versatility and universality, and the ICP-MS displays inherent disadvantages for the detection of endogenous metabolites.

In recent years, efforts have been made towards single-cell metabolite profiling using commercial organic MS.[10] Electrospray ionization (ESI) MS, with increased simplicity and versatility over CyTOF, has been developed as the detector of flow cytometry.[10b, 10d] Hundreds of metabolites have been successfully identified in single cells, providing direct information to indicate cellular behavior for potential cell subtyping and disease diagnosis. Unfortunately, although ESI-MS has been applied in single-cell proteomics,[4b] the direct monitoring of intact proteins along with metabolites in single cells remains a daunting challenge because of insufficient sensitivity and complicated matrix interference.[11] Organic mass probes for protein labeling have highly increased the sensitivity,[12] but existing probes can hardly be compatible with mass cytometry system. Mass cytometry conducting the simultaneous detection of proteins and metabolites would undoubtedly yield multi-dimensional single-cell data for more comprehensively cellular and biological understanding.

In this work, we proposed a nanoelectrospray ionization mass spectrometry (NanoESI-MS) based multi-dimensional organic mass cytometry system (Scheme 1a and Figure S1), which enabled the simultaneous analysis of multi-parameters of proteins and metabolites from single cells. A series of mass probes (MPs) were prepared by assembling rhodamine-based mass tags (RMTs) and specific antibodies on gold nanoparticles (GNPs). The RMTs, self-assembled on the GNPs through the Au–S bond (Scheme 1b) and on-line dissociated during the nanoESI process, provided the transformation of protein signals into the amplified and simplified signals of RMTs and ensured the single-cell-protein sensitivity and high throughput. Importantly, cellular metabolites could be directly detected at the same time, and the mass-to-charge ratios (m/z) and intensities of RMTs were compatible with those of the metabolites, thereby facilitating the complementary data acquisition and downstream quantitation of both proteins and metabolites. For efficient cell dispersing and ordering, a simple microfluidic chip (Figure S2) was connected to the nanoelectrospray emitter (Figure S3), which established the chip-nanoESI mass cytometry system (Scheme 1a) and further ensured the single-cell detection with high temporal throughput. The proposed organic mass cytometry was demonstrated with three ovarian cancer cell types (A2780, OVCAR-3, and SK-OV-3) and two breast cancer cell types (MCF-7 and MDA-MB-231). Cell

[*] S. Xu, Dr. Mingxia Liu, Prof. Y. Bai, Prof. H. Liu
Beijing National Laboratory for Molecular Sciences,
Key Laboratory of Bioorganic Chemistry and Molecular Engineering of Ministry of Education,
College of Chemistry and Molecular Engineering, Peking University,
Beijing 100871, P. R. China.
Tel: +86 10 6275 8198
E-mail: yu.bai@pku.edu.cn

Supporting information for this article is given via a link at the end of the document.

10.1002/anie.202009682

identification, cell typing, and cell heterogeneity analysis were achieved on the level of six surface proteins and ~100 metabolites. Heterogeneous cancer cell resistance to anticancer drugs was presented as another successful application of the organic mass cytometry.

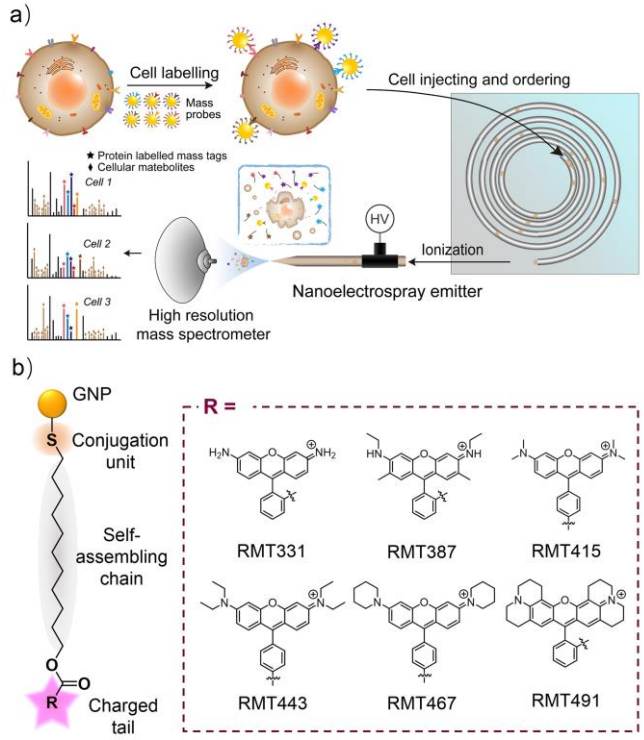

Scheme 1. (a) Schematic of the multi-dimensional chip-nanoelectrospray ionization (Chip-nanoESI) organic mass cytometry and its workflow for single-cell analysis, including cell labeling by mass probes, cell injection and ordering by the chip, dissociation and ionization by nanoESI and high-resolution MS detection. (b) Chemical structures of six rhodamine-based mass tags (RMTs: RMT331, RMT387, RMT415, RMT443, RMT467 and RMT491) self-assembled on gold nanoparticles (GNPs) by Au–S bond.

Results and Discussion

MP Preparation and On-Line Dissociation of Mass Tags. Novel MPs were developed through self-assembling of antibodies and specially designed mass tags, RMTs, on the GNPs (Figure S6), which relieved the bottlenecks of organic mass cytometric system including sensitivity, dissociation modes and compatibility of existing protein labeling probes.[8, 12b]

High specificity and sensitivity as the two key points for single-cell protein detection were ensured by the antibodies and RMTs assembled on MPs. Antibodies were utilized for target protein recognition according to their specific affinity and universality in life analysis and clinical diagnosis. Six homologous RMTs (RMT331, RMT387, RMT415, RMT443, RMT467, and RMT491, Scheme 1b and Figure S4) contributed to single-cell sensitivity because of their large quantities on GNPs and high MS response, one of which have been confirmed to achieve a limit of detection of zeptomole for free proteins in our previous work.[12d] The self-assembly quantities of antibodies and RMTs on GNPs were systematically optimized and finalized as a ratio of 1/24/9000 for GNP/antibody/RMT (Figure S7), balancing the high specific recognition towards the cell surface proteins and the large amplification by the tags. The modified GNPs were verified with obvious fluorescent signals of antibody (Figure S8-9) and fluorescence imaging of labeled cells (Figure S10), and observed to be ~20 nm in diameter with a modified corona of 2 nm thickness (Figure S11) using transmission electron microscopy (TEM) images and fluorescence imaging. A 20 min MP incubation time was employed, which further reduced the nonspecific adsorption and avoided probe endocytosis (Figure S12). Take EpCAM as an example, results from above experiments confirmed that it can be successfully detected on the single A2780 cells but not on MDA-MB-231 cells (negative control).

More importantly, the self-assembling RMTs on the GNPs were proven to be on-line dissociated during nanoESI, which was extremely significant for high-throughput mass cytometric detection. The dominant peak of the RMT443 dimers (*m/z* 628.4, *z* = 2) was confirmed as the distinguishable doubly charged peaks in the mass spectra (Figure S13a). As the most major products of Au–S bond cleavage in laser-[12b] and plasma-[13] based ionization, dimers were achieved for the first time during the nanoESI flow. The spray voltage was the most influential parameter of RMT dissociation during nanoESI process, and interesting dissociated products were obtained in the range of 1–6 kV (Figure S14). The RMT dimers (*m/z* 628.4, z = 2) were the main dissociated products at the voltage 3 kV. Higher voltage caused a higher yield of oxidative products of dissociated RMTs (e.g., *m/z* 620.4, z = 2; Figure S13b). The dissociation behavior was different from the electrospray accelerated substrate ESI-MS in which multistep oxidized derivatives presented because of the air oxygen.[12d] Simple and intensive mass reporters were achieved in this solvent-phase on-line dissociation environment. The specific doubly charged dimers were utilized as the final MS reporters which offered simple and clean spectrum with the spray voltage of 3 kV. Six homologous RMTs presented identical dissociation abilities, providing similar MS responses without cross interference (RMT331, *m/z* 516.2443; RMT387, *m/z* 572.3067; RMT415, *m/z* 600.3380; RMT443, *m/z* 628.3692; RMT467, *m/z* 652.3690; RMT491, *m/z* 676.3689; Figure S15 and Table S1). Furthermore, with the aid of crystal violet (CV) as internal standard (IS), six MPs provided good semi-quantitation results using their reporter signals above (Figure S16). The high specificity, high sensitivity, online dissociation, and simultaneous semi-quantification made the MPs ideal protein labeling probes for the organic mass cytometry.

Configuration and Performance of Chip-NanoESI Mass Cytometry. Organic mass cytometry exhibits the advantages of simplified and flexible ionization interfaces and good compatibility with various commercial mass spectrometers. The chip-nanoESI mass cytometry platform comprised four main parts (Figure S1): the cell injection system, cell ordering chip (Figure S2), home-made nanoESI device (Figure S3), and high-resolution Orbitrap mass spectrometer.

10.1002/anie.202009682

NanoESI with a tip size of 30 μm O.D. (Figure S3) was employed with a 3 kV DC voltage and an adaptive flow rate of 1 μL/min (Figure S17), which offered multiple functions including protein tag dissociation, cell lysis or rupture and ionization. To evaluate its performance, the labeled A2780 cell suspension was first attempted. A continuous low-speed vortex of cell suspension was kept during the injection to ensure the homo- and mono-dispersion of cells. To obtain results from a single cell, we found the concentration of cell suspension was crucial. As depicted in the total ion chromatograms (TICs) and extracted-ion chromatograms (EICs) (Figure S18), a high cell concentration (>10^6 cells per mL) resulted in a continuous signal from more than 1 cell and even the clogging of the emitter, and isolated peak-like signals probably from individual cells were observed when using a moderate concentration (<5×10^4 cells per mL) compatible with an MS screening speed of ~6 scans/s. The *m/z* 782.5670, assigned to the representative cell metabolite-glycerophosphocholine PC(34:1), was selected as the marker of the presence of cells. The position of peak-like signals in the EIC of *m/z* 782.5670 matched well with the TICs, further assigning the peak-like signals to single cells, and the negligible background signal between the EIC peaks indicated the absence of any interference in the solvent or between the cells (Figure S18b). However, the signals from the cell clusters frequently disturbed the single-cell detection process.

To effectively regulate cell dispersion and ordering, a five-loop microchannel chip was connected to the system. The curved square microchannel in the chip provided the regulating effect based on the Dean flow.[14] As a demonstration, the cell clusters in a high-concentration cell suspension (>10^6 cells per mL; Figure S19a) achieved mono-dispersion, and the spacing between the cells kept increasing after each cycle. For the MS-compatible concentrations (~5×10^4 cells per mL), the introduction of the microchannel chip almost completely resolved cell clusters and aligned the cells in an orderly manner (Figure S19b). This provided a series of more uniform pulse-like single-cell peaks in the TICs and EICs [PC(34:1) and *m/z* 572.3066 assigned to RMT387] (Figure 1a). For a single run, the cytometric test could last ~ 6 minutes for the analysis of more than 200 cells with a throughput of ~40 cells per min. Single cell analysis duration was ~0.32 s and the gap duration between cells was ~1 s (Figure 1a). For semi-quantification of the cellular protein tags and metabolites, the CV intensities (*m/z* 372.2433 in Figure 1b) were utilized for signal normalization, which reduced the possible variability during the ionization process (relative standard deviation (RSD) for CV = 8.7%, *n = 151*), and highlighted the intercellular differences. The normalized signals of *m/z* 782.5670 and 572.3066 from the sequentially detected *cell 1* to *cell 151* in one injection are illustrated in Figure 1c. Significant signal differentiation among the individual cells confirmed the necessity of single-cell analysis. The signal distribution within the cell populations were confirmed by ~500 cells from three tests (151, 142, and 150 cells). The percentage of A2780 cell populations with certain intensity ratios in three tests presented acceptable RSDs (11% and 6% for the highest percentages for signals *m/z* 782.5670 and 572.3066, *n = 3*; Figure 1d). All the above data indicated good reliability and stability for this organic mass cytometry platform.

More validations for the platform were conducted with two more ovarian cancer cell types (OVCAR-3, and SK-OV-3) and two breast cancer cell types (MCF-7 and MDA-MB-231) in sequence with the same workflow (Figure S5), achieving the single-cell mass spectra of five different cells (Figure S20). Furthermore, a mixed cell suspension composed of three types of cells (A2780, OVCAR-3, and MCF7) was injected and presented single cell signals as well (Figure S21a). Three unique mass spectra were extracted from three individual peaks (Figure S21b-d), which were assigned to three cell types after data analysis.

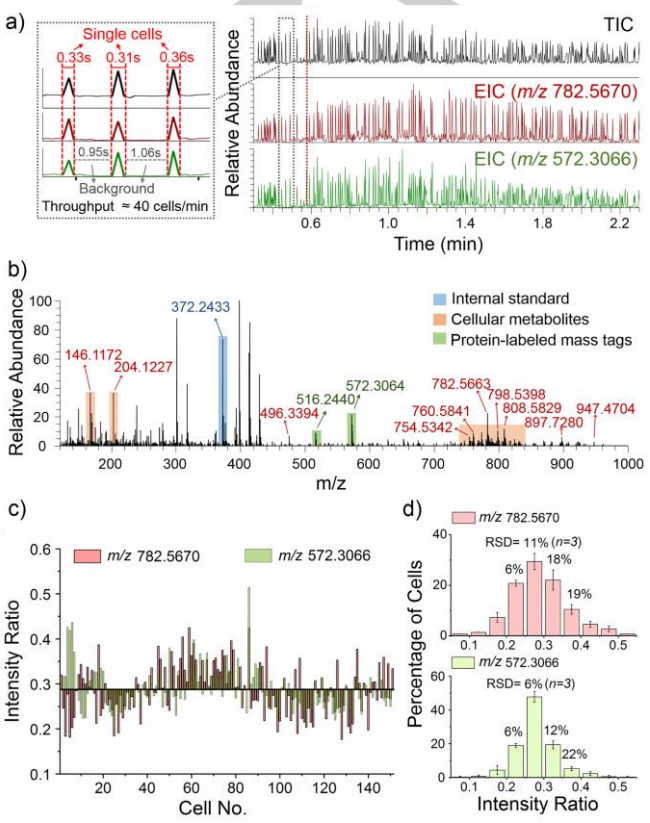

Figure 1. Performance of the chip-nanoelectrospray ionization (Chip-nanoESI) mass cytometry system. (a) Total-ion chromatogram (TIC) and extracted-ion chromatograms [EICs; glycerophosphocholine PC(34:1) of *m/z* 782.5670 and RMT387 of *m/z* 572.3066] of the cell suspension (~5×10^4 cells/mL); enlarged pulse-like peaks representing the analysis duration of individual cells (~0.32 s with ~40 cells/min). (b) A2780 single-cell mass spectrum extracted from the TIC (pulse-like peak marked with the red dotted line), providing cellular metabolite, protein tag, and internal standard (IS) signals. (c) Signal plots of *m/z* 782.5670 and 572.3066 from 151 sequential detected A2780 cells using the signal intensity ratios of target signal and IS for semi-quantification. (d) Intensity ratio distribution of *m/z* 782.5670 and 572.3066 from 151, 142, and 150 A2780 cells (most RSDs <20%, *n* = 3). RSD: relative standard deviation.

Surface Antigen Detection in Single Cells. Six antigens on cell surfaces, including three important cancer biomarkers, cancer antigen 125 (CA125), carcinoembryonic antigen (CEA), and epithelial cell adhesion molecule (EpCAM), and three commonly used cluster of differentiation (CD) antigens, CD24, CD44, and CD133, were labeled with six MPs, detected by the organic mass cytometry and then semi-quantitated.

10.1002/anie.202009682

Benefiting from the high sensitivity RMTs and large signal amplification ability of the MPs, the six cell surface antigens were successfully detected in the single-cell level (Figure 1b, green bar peaks and Figure S20, pink bar peaks). The mass reporter signals facilitated rapid identification in the complex matrix because of their characteristic doubly charged peaks and the absence of interference with the signals from cellular endogenous compounds. The semi-quantification of the surface antigens was achieved with the intensity ratios of the mass reporters and IS. The expression of the surface antigens among the five cell types and subtypes was presented with significant differences (Figure 2a). For example, as an important functional protein of epithelial carcinogenesis, EpCAM was detected in most epithelial carcinoma cell lines, including SK-OV-3, MCF-7, A2780, and OVCAR-3 but not in the MDA-MB-231 cell line.

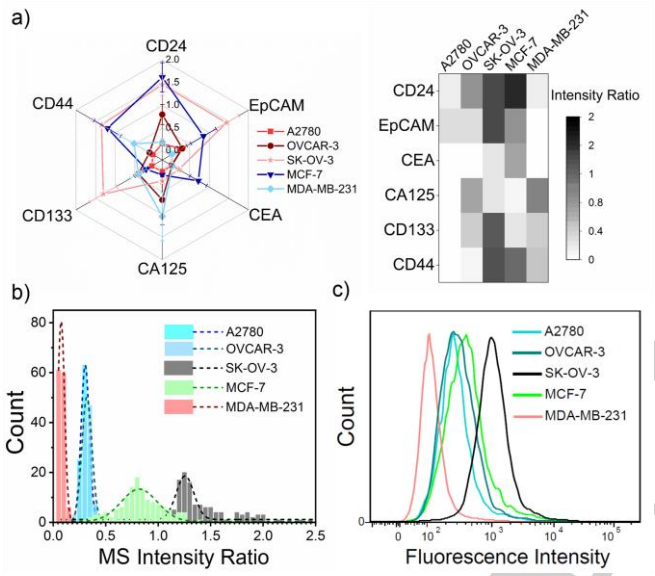

Figure 2. Single-cell surface antigen detection. (a) Spider chart and heatmap of the expression of six proteins: cluster of differentiation (CD) antigens (CD24, CD133, and CD24), epithelial cell adhesion molecule (EpCMA), carcinoembryonic antigen (CEA), cancer antigen 125 (CA125), in five cell types and subtypes (A2780, OVCAR-3, SK-OV-3, MCF-7, and MDA-MB-231). Distribution curves of the EpCAM expression in the five cell lines detected by (b) organic mass cytometry and (c) fluorescence-based flow cytometry.

To verify the semi-quantification results, gold-standard fluorescence-based flow cytometry was employed. The inherent fluorescent signals from RMTs made these MPs difunctional probes additionally for fluorescence-based flow cytometry. Therefore, the MP-labeled cells were directly subjected to commercial flow cytometry. The semi-quantification results attained by fluorescence intensity measurements (Figure S22) were well consistent with those afforded by the organic mass cytometry, such as the relative expression of EpCAM visualized by the distribution curves based on the MS intensity ratios (Figure 2b) and fluorescence intensities (Figure 2c). Furthermore, the results attained using commercial fluorescent-labeled antibodies were in satisfactory agreement with those attained with the MPs in protein semi-quantification (Figure S23), which further confirmed the specific labeling and detection of the single-cell proteins using MP-based organic mass cytometry.

These differences in cell surface antigens might be closely related to cellular function, such as proliferation and differentiation, epithelial cell adhesion, metastasis, and signaling regulation for different cell types and subtypes. As the typical indicators for cell typing,[15] different cell types and subtypes including ovarian cancer cells (A2780, OVCAR-3, and SK-OV-3) and breast cancer cells (MCF-7 and MDA-MB-231) were clearly distinguished with cellular antigen information after hierarchical clustering and visualized by principal component analysis (PCA; Figure S24), representing high sensitivity and specificity for most cell lines but a little bit confused for the identification of MDA-MB-231 cells (Most of the error scatters in Figure S24b).

Metabolite Profiling in Single Cells and Cell Typing. Apart from cell surface proteins, cellular metabolites were simultaneously identified in the single-cell mass spectra (Figure S20), taking full advantages of organic mass cytometry. Among the >500 detected peaks in the mass spectra of single cells, ~84 potential cellular metabolites were successfully identified based on the exact m/z ratio in the *m/z* 80–1200 under positive mode (Table S2). Since direct tandem MS of the metabolites from single cells was not performed because of the limited scan time (~0.32 s) for one cell, metabolite extractions of the bulk cells were analyzed to obtain the exact mass and tandem MS information to assist metabolite assignment (Figure S25). The assigned metabolites mostly included amino acids or peptides (proline, valine, threonine, leucine, creatine, glutamine, arginine, cysteinylglycine, and glutathione) and lipids [including PC, glycerophosphoglycerols (PG), glycerophosphoethanolamines (PE), triglycerides (TG), fatty acid esters. and fatty amides; Table S3]. Notably, most metabolites were extracted or released from the cytomembrane and cytoplasm (Table S4). This was mainly attributed to the short interaction time for cell lysis/rupture and metabolite extraction during electrospray.

Significant statistical differences in the cellular metabolites along with six surface antigens were observed among the different cell types and subtypes (Figure 3a and Figure S26, 27). Several amino acids and lipids displayed significant differences (Figure S28, 29), for example PC(32:1), proline, PE(P-40:6), and TG(52:2) between the A2780 and OVCAR-3 cell lines (Figure 3b). Notably, different lipid expression levels among the different cell lines were observed. Only three TGs, namely TG(50:2), TG(52:2), and TG(52:3), were present within the A2780 cells with very high intensities, while large amounts of high-intensity PCs, such as PC(38:2), PC(36:2), and PC(30:0), were found within the MCF-7 cells. Most lipids were present at much lower expression levels in the SK-OV-3 cells. The same tendencies were confirmed when unlabeled cells were analyzed (Figure S30-31), thereby eliminating the effect on metabolite detection induced by the MP addition. As the lipids perform significant functions to form cellular structures and participate in cell proliferation/differentiation and multiple signaling pathways, the lipid differences of these cancer cells were associated with different cell morphologies, generation cycles, and functions to aid cancer classification and staging.[16]

The cellular metabolites were potential biomarkers for distinguishing cells and could also be applied to assist cell type and subtype identification. With the assigned 84 metabolites, five cell types and subtypes were also successfully clustered by

10.1002/anie.202009682

hierarchical clustering and visualized in PCA (Figure S32); however, these still displayed a lower degree of discrimination for MDA-MB-231 cells (Most of the error scatters in Figure S32b).

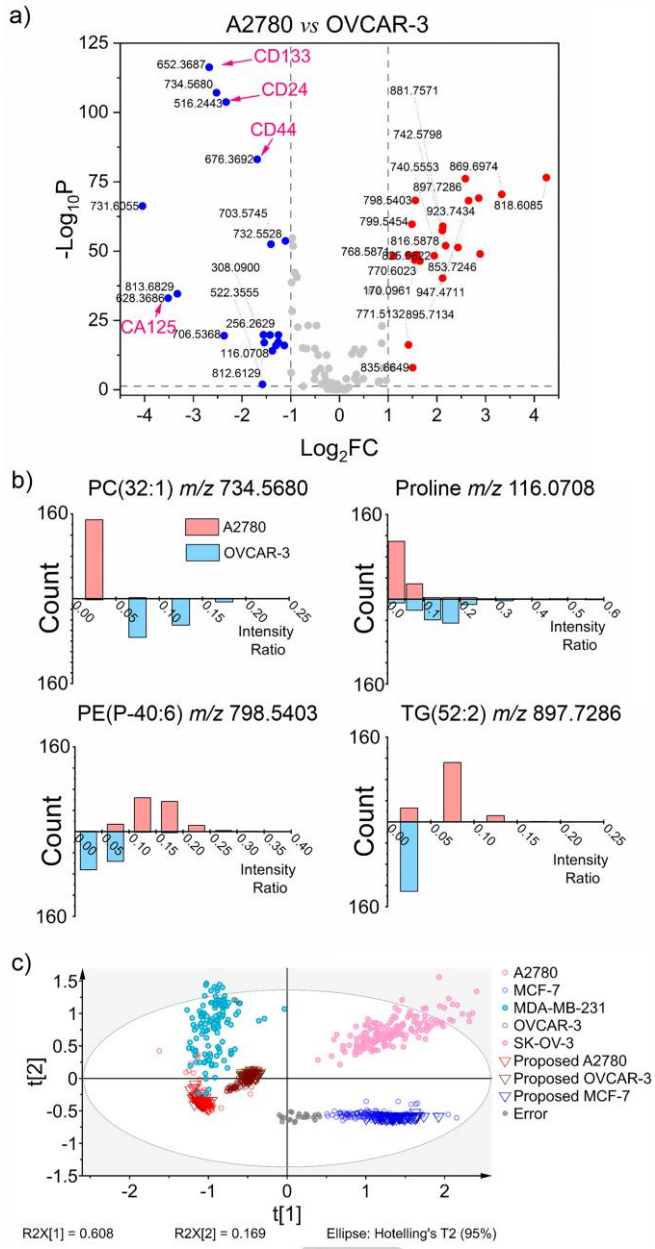

Figure 3. Metabolite profiling and cell typing. (a) Volcano plot of the correlations between the P-values and fold changes (FD) of normalized intensities for the detected mass tag and metabolite signals within A2780 and OVCAR-3 cells; differential compounds (T test, P <0.05; FD >2) depicted in red and blue dots. (b) Distribution of the representative differential metabolites: PC(32:1) (*m/z* 734.5680), proline (*m/z* 116.0708), glycerophosphoethanolamines PE(P-40:6) (*m/z* 798.5403) and triglycerides TG(52:2) (*m/z* 897.7286) in A2780 and OVCAR-3 cells. (c) Principal component analysis (PCA) of five known cell types and mixed cell sample based on the detected six mass tag and 84 metabolite signals. Cells marked based on the results of hierarchical clustering (Ward's method, square Euclidean distance), mixed cells clustered to three groups: proposed A2780 cells (red triangle scatters), proposed OVCAR-3 cells (brown triangle scatters) and proposed MCF-7 cells (blue triangle scatters).

Since the organic mass cytometry system provided rich cellular information including cell surface antigens and metabolites, a heightened cell typing for the five cell lines with both cellular proteins and metabolites was demonstrated for the first time (Figure S33). Thus, the combined protein/metabolite information resulted in the most sensitive and specific differentiation results for cell typing and identification, especially 100% for both sensitivity and specificity for the MDA-MB-231 cells (Table S5). Furthermore, the cell suspension of mixed A2780, OVCAR-3 and MCF-7 cells were also successfully distinguished with protein/metabolite information, which was preliminarily gathered to three clusters in the PCA (Orange triangle scatters in Figure S34), and highly consistent with the three identified cell clusters. After hierarchical clustering using identified cells as reference, the mixed unknown cells were clearly clustered into three cell types as 74 proposed A2780 cells, 90 proposed OVCAR-3 cells, and 87 proposed MCF-7 cells (Figure 3c), which was also consistent with the initial mixed ratios of cell suspension sample. The detection and identification of mixed sample expends the platform for more complicated and unknown system. All the above demonstrated the organic mass cytometry platform being more comprehensive, accurate and efficient for cell typing, and high potential for further biological analysis at single-cell level.

Cell Heterogeneity Analysis for Chemotherapy Resistance. Development of single-cell measurement techniques reveals cell heterogeneity among cell types and more importantly in a clonal population, which is crucial for drug resistance analysis and stem cell research in cancer therapy.[1d, 17] To investigate the drug resistant at the single-cell level, wild-type MCF-7 (wt MCF-7) cells exposed to doxorubicin were employed to induce doxorubicin-chemoresistant phenotype (DOX-res) MCF-7 cells.[18] The differentiation of DOX-res and wt MCF-7 cells at the single-cell level was conducted using our platform. The DOX-res cells presented marked differentiation in the surface antigen expression profiles, particularly the low expression level of CD24 ($CD24^{low/-}$), which has been reported as a specific marker for chemoresistant phenotypes.[17, 19] The $CD44^{+}CD24^{low/-}$ DOX-res MCF-7 cells (Figure 4a, triangle scatters) were clearly distinguished from most of the $CD44^{+}CD24^{+}$ MCF-7 cells (Figure 4a, circle scatters).

Representative metabolites with statistical differences were also singled out between the DOX-res phenotype and wt MCF-7 cells, including amino acids (arginine, glutamine, and glutamic acid) and lipids [sphingomelin SM(D34:1), PC(38:4), and PC(O-32:0); Figure 4b]. The differential metabolites could be associated with the cellular metabolic pathways and special cell morphology, which were potential indicators for the recognition of drug resistant cells and provided phenotypic evidence for the analysis of the drug resistance mechanism and the survival, differentiation, and aging of cancer cells.

Interestingly, in the results of the wt MCF-7 cell populations, a very low number of cells with relatively low CD24 expression were observed (circle scatters of $CD44^{+}CD24^{low/-}$ in Figure 4a), and the results were identical with those observed with fluorescence-based flow cytometry (Figure S35). These small clusters in the wt MCF-7 cells might be drug resistant cells and could have other stem-like features, like self-renewal and differentiation, which have been of great concern in cancer therapy.[20] The analysis of drug-resistant cancer cells further demonstrated the organic mass

cytometry system as a powerful single-cell measurement technique for cell heterogeneity analysis and cell phenotype identification and recognition.

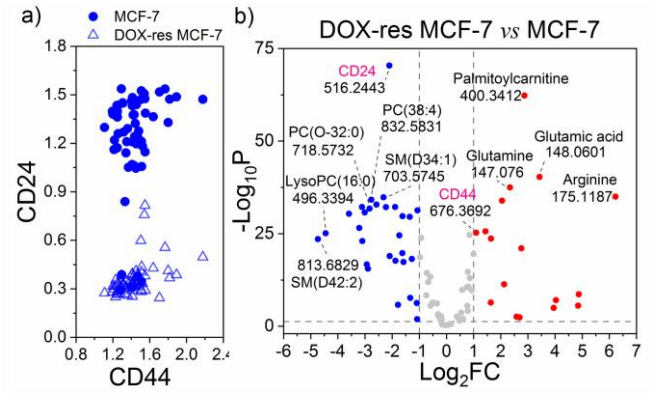

Figure 4. Chemotherapy resistance subtype analysis. (a) Scatter plot of MCF-7 (circles) and DOX-res MCF-7 (triangles) cells based on CD24 and CD44 expression. (b) Volcano plot of the correlations between the P-values and fold changes (FD) of normalized intensities for the detected mass tag and metabolite signals within MCF-7 and DOX-res MCF-7 cells, differential compounds (T test, P <0.05; FD >2) illustrated as red and blue dots.

Conclusion

In summary, a multi-dimensional organic mass cytometry platform was developed for the simultaneous analysis of single-cell proteins and metabolites. Sufficient sensitivity for single-cell protein detection was achieved with six mass tags-RMTs assembled on GNPs for signal transformation and amplification. The online dissociation of RMTs and specific recognition using antibodies provided the highly sensitive and specific semi-quantification of six cell surface antigens at the single-cell level. A facile integrated setup comprising cell injection, cell ordering, and ionization was established, which could be easily coupled with a high-resolution mass spectrometer for cytometric measurement. Cell suspension was analyzed with a throughput of ~40 cells per minute, providing six protein parameters and ~100 metabolite parameters at single-cell resolution. Cancer cell phenotypes and substantial heterogeneity were better distinguished and identified based on the comprehensive cell surface antigens and cellular metabolites, achieving more than 95% sensitivity and specificity for cell typing. Moreover, the drug resistant and stem-like cells within MCF-7 were recognized based on antigen markers, and metabolic differences were found for further drug resistance analysis and stem cell research. Combining significant protein targets with hundreds of downstream metabolites, the multi-dimensional mass cytometry offers a high possibility for the deep understanding of fundamental biological processes such as differentiation, aging, and pathopoiesis at single-cell level.

Acknowledgements

This work was financially supported by the National Natural Science Foundation of China (21874003, 21527809, and 21728501), National Key R&D Program of China (2016YFF0100303) and Beijing Natural Science Foundation Essential Research Project (Z170002).

Keywords: mass cytometry • single-cell heterogeneity• mass tags • surface protein • metabolites

[1] a) A. Colman-Lerner, A. Gordon, E. Serra, T. Chin, O. Resnekov, D. Endy, C. G. Pesce, R. Brent, *Nature* **2005**, *437*, 699-706; b) L. Bintu, J. Yong, Y. E. Antebi, K. McCue, Y. Kazuki, N. Uno, M. Oshimura, M. B. Elowitz, *Science* **2016**, *351*, 720-724; c) M. Yazawa, B. Hsueh, X. Jia, A. M. Pasca, J. A. Bernstein, J. Hallmayer, R. E. Dolmetsch, *Nature* **2011**, *471*, 230-234; d) B. M. Seo, M. Miura, S. Gronthos, P. M. Bartold, S. Batouli, J. Brahim, M. Young, P. G. Robey, C. Y. Wang, S. T. Shi, *Lancet* **2004**, *364*, 149-155.

[2] a) D. Wang, S. Bodovitz, *Trends Biotechnol.* **2010**, *28*, 281-290; b) A. Schmid, H. Kortmann, P. S. Dittrich, L. M. Blank, *Curr. Opin. Biotechnol.* **2010**, *21*, 12-20.

[3] a) E. Z. Macosko, A. Basu, R. Satija, J. Nemesh, K. Shekhar, M. Goldman, I. Tirosh, A. R. Bialas, N. Kamitaki, E. M. Martersteck, J. J. Trombetta, D. A. Weitz, J. R. Sanes, A. K. Shalek, A. Regev, S. A. McCarroll, *Cell* **2015**, *161*, 1202-1214; b) A. P. Patel, I. Tirosh, J. J. Trombetta, A. K. Shalek, S. M. Gillespie, H. Wakimoto, D. P. Cahill, B. V. Nahed, W. T. Curry, R. L. Martuza, D. N. Louis, O. Rozenblatt-Rosen, M. L. Suva, A. Regev, B. E. Bernstein, *Science* **2014**, *344*, 1396-1401; c) P. Zhang, X. Han, J. Yao, N. Shao, K. Zhang, Y. Zhou, Y. Zu, B. Wang, L. Qin, *Angew. Chem. Int. Ed.* **2019**, *58*, 13700-13705.

[4] a) A. J. Hughes, D. P. Spelke, Z. Xu, C.-C. Kang, D. V. Schaffer, A. E. Herr, *Nat. Methods* **2014**, *11*, 749-755; b) Y. Zhu, G. Clair, W. B. Chrisler, Y. Shen, R. Zhao, A. K. Shukla, R. J. Moore, R. S. Misra, G. S. Pryhuber, R. D. Smith, C. Ansong, R. T. Kelly, *Angew. Chem. Int. Ed.* **2018**, *57*, 12370-12374.

[5] a) R. Zenobi, *Science* **2013**, *342*, 1243259; b) M. Fessenden, *Nature* **2016**, *540*, 153-155.

[6] a) T. J. Comi, T. D. Do, S. S. Rubakhin, J. V. Sweedler, *J. Am. Chem. Soc.* **2017**, *139*, 3920-3929; b) L. Zhang, A. Vertes, *Angew. Chem. Int. Ed.* **2018**, *57*, 4466-4477.

[7] M. H. Spitzer, G. P. Nolan, *Cell* **2016**, *165*, 780-791.

[8] R. Liu, S. Zhang, C. Wei, Z. Xing, S. Zhang, X. Zhang, *Acc. Chem. Res.* **2016**, *49*, 775-783.

[9] a) S. C. Bendall, E. F. Simonds, P. Qiu, E.-a. D. Amir, P. O. Krutzik, R. Finck, R. V. Bruggner, R. Melamed, A. Trejo, O. I. Ornatsky, R. S. Balderas, S. K. Plevritis, K. Sachs, D. Pe'er, S. D. Tanner, G. P. Nolan, *Science* **2011**, *332*, 687-696; b) C. Boettcher, S. Schlickeiser, M. A. M. Sneeboer, D. Kunkel, A. Knop, E. Paza, P. Fidzinski, L. Kraus, G. J. L. Snijders, R. S. Kahn, A. R. Schulz, H. E. Mei, E. M. Hol, B. Siegmund, R. Glauben, E. J. Spruth, L. D. de Witte, J. Priller, N. B. B. Psy, *Nat. Neurosci.* **2019**, *22*, 78-90.

[10] a) E. K. Neumann, T. J. Comi, S. S. Rubakhin, J. V. Sweedler, *Angew. Chem. Int. Ed.* **2019**, *58*, 5910-5914; b) H. Yao, H. Zhao, X. Zhao, X. Pan, J. Feng, F. Xu, S. Zhang, X. Zhang, *Anal. Chem.* **2019**, *91*, 9777-9783; c) Z. Yin, X. Cheng, R. Liu, X. Li, L. Hang, W. Hang, J. Xu, X. Yan, J. Li, Z. Tian, *Angew. Chem. Int. Ed.* **2019**, *58*, 4541-4546; d) Q. Huang, S. Mao, M. Khan, L. Zhou, J. M. Lin, *Chem. Commun.* **2018**, *54*, 2595-2598; e) Q. Huang, S. Mao, M. Khan, W. Li, Q. Zhang, J. M. Lin, *Chem. Sci.* **2020**, *11*, 253-256.

[11] G. Li, S. Yuan, S. Zheng, Y. Liu, G. Huang, *Anal. Chem.* **2018**, *90*, 3409-3415.

[12] a) J. R. Lee, A. Lee, S. K. Kim, K. P. Kim, H. S. Park, W.-S. Yeo, *Angew. Chem. Int. Ed.* **2008**, *47*, 9518-9521; b) Y. Wang, R. Du, L. Qiao, B. Liu, *Chem. Commun.* **2018**, *54*, 9659-9662; c) W. Ma, S. Xu, H. Nie, B. Hu, Y. Bai, H. Liu, *Chem. Sci.* **2019**, *10*, 2320-2325; d) S. Xu, W. Ma, Y. Bai, H. Liu, *J. Am. Chem. Soc.* **2019**, *141*, 72-75.

[13] R. K. Manova, S. Joshi, A. Debrassi, N. S. Bhairamadgi, E. Roeven, J. Gagnon, M. N. Tahir, F. W. Claassen, L. M. W. Scheres, T. Wennekes, K. Schroen, T. A. van Beek, H. Zuilhof, M. W. F. Nielen, *Anal. Chem.* **2014**, *86*, 2403-2411.

[14] E. W. M. Kemna, R. M. Schoeman, F. Wolbers, I. Vermes, D. A. Weitz, A. van den Berg, *Lab Chip* **2012**, *12*, 2881-2887.

[15] N. Samusik, Z. Good, M. H. Spitzer, K. L. Davis, G. P. Nolan, *Nat. Methods* **2016**, *13*, 493-496.

[16] a) Y. Sunami, A. Rebelo, J. Kleeff, *Cancers* **2017**, *10*, 3; b) E. Currie, A. Schulze, R. Zechner, T. C. Walther, R. V. Farese, Jr., *Cell Metab.* **2013**, *18*, 153-161.

[17] K. Meirelles, L. A. Benedict, D. Dombkowski, D. Pepin, F. I. Preffer, J. Teixeira, P. S. Tanwar, R. H. Young, D. T. MacLaughlin, P. K. Donahoe, X. Wei, *Proc. Natl. Acad. Sci. U. S. A.* **2012**, *109*, 2358-2363.

10.1002/anie.202009682

[18] P. C. Marinello, C. Pannis, T. N. Xavier Silva, R. Binato, E. Abdelhay, J. A. Rodrigues, A. L. Mencalha, N. M. Dias Lopes, R. C. Luiz, R. Cecchini, A. L. Cecchini, *Scientific Reports* **2019**, *9*.
[19] a) E. Amir, A. Ocana, O. Freedman, M. Clemons, B. Seruga, *Nat. Rev. Clin. Oncol.* **2010**, *7*, 79-80; b) S. Liu, Y. Cong, D. Wang, Y. Sun, L. Deng, Y. Liu, R. Martin-Trevino, L. Shang, S. P. McDermott, M. D. Landis, S. Hong, A. Adams, R. D'Angelo, C. Ginestier, E. Charafe-Jauffret, S. G. Clouthier, D. Birnbaum, S. T. Wong, M. Zhan, J. C. Chang, M. S. Wicha, *Stem Cell Rep.* **2014**, *2*, 78-91; c) A. M. Calcagno, C. D. Salcido, J.-P. Gillet, C.-P. Wu, J. M. Fostel, M. D. Mumau, M. M. Gottesman, L. Varticovski, S. V. Ambudkar, *J. Natl. Cancer Inst.* **2010**, *102*, 1637-1652.
[20] G. Farnie, F. Sotgia, M. P. Lisanti, *Oncotarget* **2015**, *6*, 30472-30486.

10.1002/anie.202009682

WILEY-VCH

Entry for the Table of Contents

RESEARCH ARTICLE

A multi-dimensional organic mass cytometry was established, enabling simultaneous monitoring of six cell surface proteins and ~100 metabolites (including lipids and amino acids) at single-cell level with a throughput of ~40 cells/min. More comprehensive protein and metabolite parameters were applied for heterogeneous single-cell analysis, including cell typing, chemotherapy resistance, and stemness recognition.

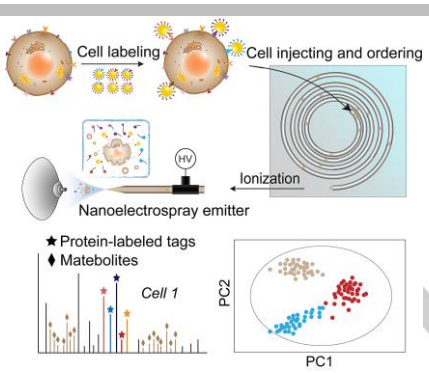

Shuting Xu, Mingxia Liu, Yu Bai, and Huwei Liu*

Page No. – Page No.

Multi-Dimensional Organic Mass Cytometry: Simultaneous Analysis of Proteins and Metabolites on Single Cells